Efficiency of Erbium 3-μm Crystal and Fiber Lasers

M. Pollnau, R. Spring, Ch. Ghisler, S. Wittwer, W. Lüthy, and H. P. Weber, *Fellow, IEEE*

***Abstract*— The population dynamics of erbium 3-μm crystal and fiber lasers are compared experimentally and theoretically. Laser slope efficiencies of 40 % in Er:$LiYF_4$ and 23% in a fluorozirconate fiber are experimentally demonstrated under Ti:sapphire pumping. These are both to our knowledge the highest values reported so far for the different host geometries. On the basis of the excitation and loss mechanisms, the best pump wavelengths are determined to be 970 nm in $LiYF_4$ and 791 nm in a fluorozirconate fiber. The theoretical limit of the slope efficiency with respect to absorbed pump power is redefined as depending on the major population mechanisms of the system. Calculated values are 56% in Er:$LiYF_4$ and 27% in a fluorozirconate fiber.**

PACS number(s): 42.55.Rz, 42.55.Wd, 42.60.Lh, 78.45.+h.

I. Introduction

POSSIBLE surgical applications [1] due to the high absorption of 3-μm radiation in water have stimulated investigations of laser sources in this wavelength range. Promising candidates for efficient laser operation at 3 μm are erbium-doped crystal and fiber lasers. Erbium crystal lasers deliver high output powers [2], [3] up to 1 W. In erbium-doped fluoride single-mode fibers, an output power of 150 mW has recently been demonstrated [4]. For surgical applications, the output of a crystal laser has to be fiber coupled with efficiency losses in order to provide the laser beam at the location of the application. This is not necessary with the fiber laser, but the output power obtained from fibers has as yet not been sufficient for surgery. A compromise is the fiber transmission of the pump to a crystalline laser head [5], but heat removal from the laser head becomes a problem at high output powers.

The erbium level scheme and the relevant transitions are displayed in Fig. 1 for crystal hosts and in Fig. 2 for fiber hosts. The $^4I_{11/2}$ upper laser level of the 3-μm transition has a shorter lifetime than the $^4I_{13/2}$ lower laser level. Stimulated emission in the cw regime has nevertheless been obtained in several host materials. Four mechanisms are responsible for this behavior: 1) The Stark splitting and Boltzmann population of the $^4I_{11/2}$ and $^4I_{13/2}$ multiplets support inversion on the long-wavelength side of the emission. 2) A moderate multiphonon quenching of the $^4I_{11/2}$ upper laser level and a small branching ratio on the laser transition hinders the $^4I_{13/2}$ lower laser level from being significantly populated [6]. 3) An interionic upconversion process depletes the lower laser level [7]. 4) An excited-state absorption (ESA) depletes the lower laser level [8]. These mechanisms contribute in different ways and degrees to the establishment of cw inversion depending on host geometry (crystal or fiber), its line-width-broadening

Manuscript received September 18, 1995; revised December 13, 1995. This work was supported in part by the Swiss Priority Program "Optique."

The authors are with the Institute of Applied Physics, University of Bern, Sidlerstrasse 5, CH-3012 Bern, Switzerland.

Publisher Item Identifier S 0018-9197(96)02560-2.

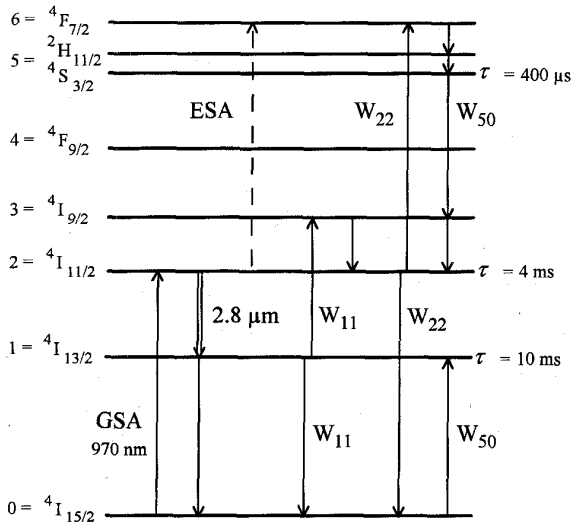

Fig. 1. Energy level scheme of the 2.8-μm Er^{3+}:$LiYF_4$ laser indicating that interionic processes dominate the excitation mechanisms of the laser levels of the 2.8-μm transition. ESA is significant only under a tight pump focus. The given lifetimes are mean values approximated from data published in literature.

mechanisms and phonon energies, dopant concentration, and special arrangements such as colasing or energy transfer to codopants.

In this paper, the population dynamics of erbium 3-μm crystal and fiber lasers are compared in detail. Laser slope efficiencies of 40% in a crystal and 23% in a fiber are experimentally obtained. These are both to our knowledge the highest values reported so far for each host geometry. On the basis of the excitation mechanisms, the best pump wavelengths and the theoretical limits for the slope efficiencies are determined and compared to the experiments. Results are different for crystals and fibers.

II. Experimental

The input-output characteristics of Er^{3+}(15 at.%):$LiYF_4$ and Er^{3+}(1000 ppm mol) in a fluorozirconate single-mode fiber are investigated under excitation by an Ar^+-laser-pumped Ti:sapphire laser.

The most efficient excitation of the crystal laser is direct pumping of the $^4I_{11/2}$ upper laser level [9], [10] in the 970-nm pump band. The pump beam is chopped with frequency 17 Hz and duty cycle 33%, which provides an excitation time of 20 ms. In view of the effective lifetimes (including interionic processes) of the laser levels in the order of 1 ms in $LiYF_4$ [10], the laser operates practically in the cw regime

TABLE I
(a) EXPERIENTAL DATA AND THE OPTICAL PROPERTIES OF THE ACTIVE MEDIA. PARAMETERS ARE PARTLY TAKEN FROM [4], [10]. UPCONVERSION PARAMETERS ARE TAKEN FROM [17]. (b) TYPICAL PARAMETERS OF LASER EXPERIMENTS WITH A CRYSTAL OR A FIBER AS AN ACTIVE MEDIUM

	Er(15%):$LiYF_4$	Er(1000 ppm mol):ZBLAN
(a) experimental data	this paper	[4]
dopant concentration	$N_d = 2.1 \times 10^{21}$ cm^{-3}	$N_d = 1.8 \times 10^{19}$ cm^{-3}
length	$\ell = 0.45$ cm	$\ell = 480$ cm
mode radius	r = 40 μm	r = 3.25 μm
pump wavelength	$\lambda_p = 970$ nm	$\lambda_p = 791$ nm
GSA cross section	$\sigma_0 = 1 \times 10^{-20}$ cm^2	$\sigma_0 = 4.7 \times 10^{-22}$ cm^2
upconversion / ESA from $^4I_{13/2}$	$W_{11} = 3.0 \times 10^{-17}$ cm^3/s	$\sigma_1 = 1.0 \times 10^{-21}$ cm^2
upconversion / ESA from $^4I_{11/2}$	$W_{22} = 1.8 \times 10^{-17}$ cm^3/s	$\sigma_2 = 2.0 \times 10^{-22}$ cm^2
laser wavelength	$\lambda_l = 2.81$ μm	$\lambda_l = 2.71$ μm
branching ratio from upper to lower laser level	$\beta_{21} = 0.39$	$\beta_{21} = 0.39$
emission cross section	$\sigma_{21} = 3 \times 10^{-20}$ cm^2	$\sigma_{21} = 5.7 \times 10^{-21}$ cm^2
Boltzmann factors	$b_1 = 0.113$, $b_2 = 0.200$	Er:$LiYF_4$ data assumed
mirror transmission	T = 1.2 % on each side	T = 68 % on each side
optical resonator length	$\ell_{opt} = 7.7$ cm	$\ell_{opt} = 720$ cm
experimental slope efficiency	$\eta_{slope} = 40$ %	$\eta_{slope} = 23$ %
theoretical limit	$\eta_{slope} = 56$ %	$\eta_{slope} = 27$ %
(b) typical values ($P_{in} = 200$ mW)		
excitation density N_{exc}	4×10^{19} cm^{-3}	1×10^{19} cm^{-3}
GSA rate	2×10^{22} cm^{-3}s^{-1}	1×10^{22} cm^{-3}s^{-1}
ESA rate	4×10^{20} cm^{-3}s^{-1}	1×10^{22} cm^{-3}s^{-1}
interionic rate	5×10^{22} cm^{-3}s^{-1}	3×10^{19} cm^{-3}s^{-1}

[11]. Under true cw excitation, the slope efficiency is not changed. The pump beam is focused into the crystal with a lens of focal length $f = 65$ mm. The pump-beam waist at the crystal front surface is approximately $r = 40$ μm. Similar laser results are obtained with focal length $f = 50$ mm. The effective ground-state-absorption (GSA) cross section at the 973-nm pump wavelength is 6×10^{-21} cm^2 [12]. More than 99% of the pump power are absorbed within the crystal of length 4.5 mm. The nearly hemiconcentric resonator consists of a plane input mirror and a mirror with radius 75 mm. The $LiYF_4$ sample is mounted on a water-cooled copper block and is placed close to the input mirror. The laser-beam waist at the crystal front face is approximately 50 μm. Both mirrors have a nonoptimized transmission $T = 1.2\%$ at 2.81 μm. The 2.81-μm laser radiation is emitted in equal parts on both sides of the resonator. This is verified by placing identical beam splitters on each side outside of the resonator, pumping through one of them, and measuring simultaneously the output powers reflected by the beam splitters.

In contrast to the crystal laser, the fiber laser is operated in a cascade regime on the transitions $^4I_{11/2} \rightarrow {}^4I_{13/2}$ at 2.71 μm and $^4S_{3/2} \rightarrow {}^4I_{9/2}$ at 1.72 μm, see Fig. 2. Here the excitation wavelength of 791 nm proved to be optimum. The reason for this will be explained later. Excitation is truly cw. The fiber experiments have been explained in detail in [4]. The experimental data and the optical properties of the active media are summarized in Table I(a).

The input-output curves are shown in Fig. 3. Slope efficiencies with respect to absorbed pump power of 40% in the crystal experiment and 23% in the fiber experiment are obtained. Note that the slope efficiency in the crystal experiment exceeds the stokes limit of $\eta_{st} = \lambda_p/\lambda_l = 35\%$. λ_p and λ_l denote pump and laser wavelength, respectively. The saturation of the output power that has occurred so far in erbium 3-μm fiber lasers [13]–[16] due to competitive lasing at 850 nm [8] is overcome in the cascade-lasing regime of Fig. 2.

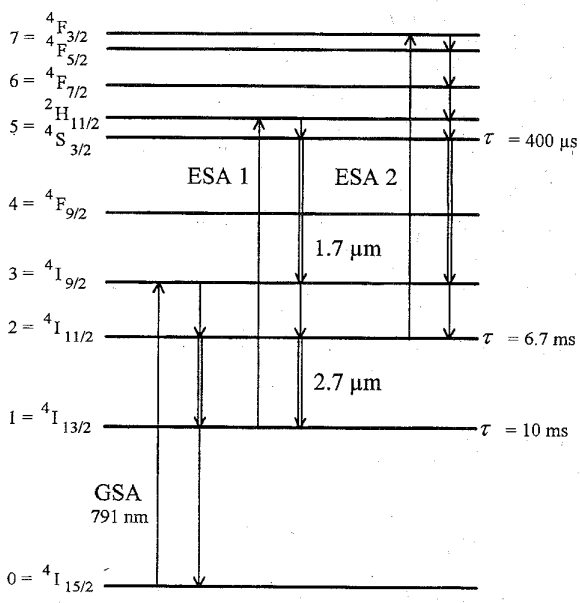

Fig. 2. Energy level scheme of the 2.7-μm Er^{3+} cascade laser in fluorozirconate fibers indicating that ESA processes dominate the excitation mechanisms of the laser levels of the 2.7-μm transition. The given lifetimes are mean values approximated from data published in literature.

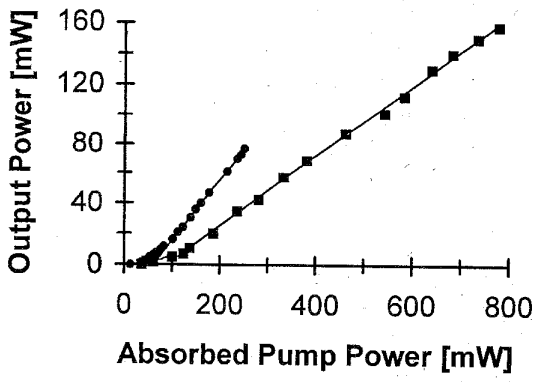

Fig. 3. Input-output curves of the 3-μm lasers in Er^{3+}:$LiYF_4$ (circles) pumped at 970 nm and in a fluorozirconate fiber (squares) pumped at 791 nm. Slope efficiencies are 40% and 23%, respectively.

III. POPULATION MECHANISMS IN CRYSTALS AND FIBERS

Generally, there are a lot of host materials that allow the implementation of erbium as a lasing dopant. Computer simulations have shown, however, that the lifetime of the $^4I_{11/2}$ upper laser level is a crucial parameter for the achievement of a high output power [10]. The multiphonon quenching of the lifetime of the upper laser level, therefore, reduces the availability mainly to fluoride materials that provide smaller maximum-phonon energies than oxide materials. Our experiments in $LiYF_4$ and fluorozirconate fibers (Section II) have, in general, confirmed the result of the simulations. For the

following, we concentrate our investigation on fluoride host materials.

A. Common Mechanisms

Stark splitting and a moderate multiphonon quenching lead to the establishment of cw inversion in both fluoride crystals and fibers. The Stark splitting in fibers is covered by the inhomogeneous broadening of the line shapes. It contributes to inversion, however, in a similar way as in crystals. Thanks to small phonon energies the lifetimes τ_i of upper and lower laser level (see Figs. 1 and 2) are comparable. The branching ratio β_{21} from upper to lower laser level given in Table I(a) leads to a weak feeding of the $^4I_{13/2}$ lower laser level. The ratio of population densities N_i times Boltzmann factors b_i of upper and lower Stark laser level without laser operation [6]

$$(b_2N_2)/(b_1N_1) = b_2\tau_2/(\beta_{21}b_1\tau_1) > 1 \tag{1}$$

ensures population inversion in the cw regime [6], [10].

So far, interionic upconversion and ESA processes have been neglected. The maximum slope efficiency η_{slope} for the output at laser wavelength λ_l when pumping at wavelength λ_p is given by the product of stokes efficiency η_{st} and quantum efficiency η_q

$$\eta_{\text{st}} = \lambda_p/\lambda_l \tag{2}$$

$$\eta_{\text{q}} = n_l/n_p \tag{3}$$

$$\eta_{\text{slope}} = \eta_{\text{st}}\eta_q = (\lambda_p/\lambda_l)(n_l/n_p). \tag{4}$$

n_l and n_p denote the number of laser and pump photons, respectively. Direct pumping of the $^4I_{11/2}$ upper laser level at 970 nm ($\eta_{\text{st}} = 0.35$) and conversion of each pump photon into one laser photon at 2.8 μm ($\eta_q = 1$) provides the highest slope efficiency of 35%.

If several transitions j are contributing to the pump absorption, the absorbed pump power P_{abs}, the relative efficiency ε_i of the absorption from level i, and the pump rate R_i from level i on the transition with absorption cross section σ_i are given by

$$P_{\text{abs}} = P_{\text{in}}[1 - \exp\{-\Sigma_j(\sigma_j N_j)\ell\}], \tag{5}$$

$$\varepsilon_i = \sigma_i N_i/\Sigma_j(\sigma_j N_j), \tag{6}$$

$$R_i = \varepsilon_i\eta_m P_{\text{abs}}\lambda_p/(hc\pi r^2\ell) \tag{7}$$

with η_m, the geometrical overlap between pump and laser mode, h, Planck's constant, and c, the vacuum speed of light. The other parameters are explained in Table I(a). If only GSA is present, the excitation density N_e can be estimated from (5)–(7) with

$$R_0 = \eta_m P_{\text{in}}[1 - \exp\{-\sigma_0(N_d - N_e)\ell\}]\lambda_p/(hc\pi r^2\ell),$$
$$dN_e/dt = R_0 - N_e/\tau_e = 0 \Rightarrow N_e = R_0\tau_e. \tag{8}$$

Assuming an input power $P_{\text{in}} = 200$ mW, a perfect overlap $\eta_m = 1$, excited-state lifetimes typically in the order of $\tau_e = 1$ ms, dopant concentration N_d and other values as given in Table I(a), we obtain $R_0 = 2 \times 10^{22}$ cm^{-3}s^{-1} and $N_e = 4 \times 10^{19}$ cm^{-3} in crystals. In fibers, typical results are $R_0 = 1 \times 10^{22}$ cm^{-3}s^{-1} and $N_e = 1 \times 10^{19}$ cm^{-3}. Despite the different dimensions of crystals and fibers, the density of excited ions is comparable.

B. Differences

The inclusion of interionic processes and ESA radically modifies this view. The contribution of the characteristic population processes is different. With (6) and (7), the relative rate of an ESA process compared to a GSA process with the same cross section σ is

$$R_{\text{ESA}}/R_{\text{GSA}} = \varepsilon_{\text{ESA}}/\varepsilon_{\text{GSA}} = N_e/(N_d - N_e). \tag{9}$$

With the value for N_e estimated above a ratio of 0.02 is obtained in highly-doped crystals which indicates that ESA is negligible. Computer simulations of erbium-doped 3-μm crystal lasers [10] have in fact confirmed experimental results [2] that ESA has practically no influence in crystals if the pump intensity is not high enough to induce ground-state bleaching. This is practically the case under diode pumping of crystals with Er^{3+} conc. >10%. On the other hand, interionic processes with typical parameters [17] $W_{\text{IP}} = 3\times 10^{-17}$ cm^{3}s^{-1} amount in interionic-transition rates $R_{\text{IP}} = W_{\text{IP}}N_e^2 = 5 \times 10^{22}$ cm^{-3}s^{-1} which are in the range of the pump rate. This underlines the dominant role of interionic processes at a dopant concentration of 2×10^{21} cm^{-3}.

In low-doped fibers, the ratio of (9) is in the order of unity. In addition, the inhomogeneous broadening of the line shapes leads to a good overlap between the spectra of GSA and ESA. ESA processes have, therefore, a serious impact on the population mechanisms. Interionic processes suffer from the circumstance that the dopant concentration in 1000-ppm-mol erbium-doped fibers is smaller by a factor of 100. This reduces the probability of two excitations to meet at nearest-neighbor distance via diffusion. The assumption of a constant ratio W_{IP}/N_d would result in typical interionic parameters $W_{\text{IP}} = 3 \times 10^{-19}$ cm^{3}s^{-1} and rates $R_{\text{IP}} = 3 \times 10^{19}$ cm^{-3}s^{-1}. This rough estimation demonstrates the orders of magnitude of the relevant processes: Interionic processes are negligible at a dopant concentration $N_d = 1.8 \times 10^{19}$ cm^{-3}. The typical values for the excitation density and the rates of the characteristic processes are summarized in Table I(b).

IV. Crystal Hosts: Interionic-Energy-Transfer Domain

The investigations of Section III have shown that ion-ion interactions dominate the population dynamics of highly-doped erbium 3-μm crystal lasers. Direct pumping of the $^4I_{11/2}$ upper laser level at 970 nm is the most efficient excitation [9], [10]. Interionic processes do not influence this fact because of the conservation of energy. The slope efficiency is given by (4): $\eta_{\text{slope}} = \eta_{\text{st}} \times \eta_q = 0.35\eta_q$. Pumping of an upper state and cross relaxation into the $^4I_{11/2}$ upper laser level gives $\eta_q' = 2\eta_q$, but the pump-level energy must be at least twice the energy of the upper laser level in order to allow for the cross relaxation, thus giving $\eta_{\text{st}}' = 0.5\eta_{\text{st}}$. The

result is $\eta_{\text{slope}} = \eta'_{\text{st}} \times \eta'_q = 0.35\ \eta_q$. Pumping of the $^4I_{13/2}$ lower laser level and upconversion into the $^4I_{11/2}$ upper laser level [18], [19] requires two pump photons at 1.5 μm for one excitation to be upconverted to the upper laser level. This results in $\eta_{\text{slope}} = \eta''_{\text{st}} \times \eta''_q = 0.54 \times 0.5\eta_q = 0.27\eta_q$.

After the lasing process, however, ion-ion interactions have an impact on slope efficiency. We have demonstrated a slope efficiency of 40% clearly exceeding the limit of 35% predicted by (4) due to energy recycling via upconversion W_{11}, see Fig. 1. The simple model of Fig. 1 gives a deeper understanding of the recycling process and the expected slope efficiency.

We assume that the $^4I_{13/2}$ lower laser level is depleted exclusively via upconversion W_{11}. Half of its population is recycled via multiphonon relaxation into the $^4I_{11/2}$ upper laser level. A second upconversion process W_{22} which, however, is undesired depletes the $^4I_{11/2}$ upper laser level and populates the $^4S_{3/2}$ level. The cross relaxation W_{50} distributes the energy into the $^4I_{11/2}$ upper laser level via multiphonon relaxation and directly into the $^4I_{13/2}$ lower laser level. The green erbium laser originating from $^4S_{3/2}$ is an excellent monitor for this cross relaxation [20]. The parameter W_{50} is large enough to allow for the recycling of most of the $^4S_{3/2}$ population (compare [10] and [20]). Thus, the upconversion W_{22} introduces two connected paths (see Fig. 1): first $^4I_{11/2} \rightarrow {}^4F_{7/2} \rightarrow {}^4S_{3/2} \rightarrow {}^4I_{9/2} \rightarrow {}^4I_{11/2}$ which does not affect the population of the $^4I_{11/2}$ upper laser level if the involved processes are fast enough, and second $^4I_{11/2} \rightarrow {}^4I_{15/2} \rightarrow {}^4I_{13/2}$ which transfers one excitation from upper to lower laser level. The rate equations for the population densities N_i and the photon density ϕ in this model are

$$dN_2/dt = R_0 - (b_2N_2 - b_1N_1)\sigma_{21}c\phi + W_{11}N_1^2 - W_{22}N_2^2, \quad (10)$$

$$dN_1/dt = (b_2N_2 - b_1N_1)\sigma_{21}c\phi - 2W_{11}N_1^2 + W_{22}N_2^2, \quad (11)$$

$$N_d = N_0 + N_1 + N_2 \quad (12)$$

$$d\phi/dt = \{\ell(b_2N_2 - b_1N_1)\sigma_{21} + 0.5\ln[(1-T)(1-L)]\}c\phi/\ell_{\text{opt}} \quad (13)$$

with resonator losses L and the parameters of Table I(a). In the steady-state regime, the combination of (10)–(13) yields

$$c\phi = +2\ell X[2 - (b_1/b_2)^2(W_{22}/W_{11})]R_0 - 2(b_1/b_2)W_{22}/(b_2\sigma_{21}W_{11}^{1/2})R_0^{1/2} - 2\ell X W_{22}/(b_2\sigma_{21})^2, \quad (14)$$

where

$$X = -1/\ln[(1-T)(1-L)] \quad (15)$$

is a positive expression. The last term in (14) indicates a threshold behavior due to resonator losses and depletion of the $^4I_{11/2}$ upper laser level via upconversion. The other terms are pump dependent. The term which is proportional to $R_0^{1/2}$ has only a small influence with the set of parameters given in Table I(a) and neglecting resonator losses L. The output power P_{out} is

$$P_{\text{out}} = 0.5c\phi(hc/\lambda_l)\pi r^2 T. \quad (16)$$

Combination of (7), (14), and (16) then yields the slope efficiency

$$\eta_{\text{slope}} = dP_{\text{out}}/dP_{\text{abs}} = (\lambda_p/\lambda_l)\eta_m TX[2 - (b_1/b_2)^2(W_{22}/W_{11})]. \quad (17)$$

We define here the theoretical limit for the slope efficiency as depending on the population mechanisms of the system. Losses are negligible, i.e., $TX = 1$, and the overlap of pump and laser mode is perfect: $\eta_m = 1$. In the absence of upconversion W_{22}, the theoretical limit for the slope efficiency derived from (17) is $\eta_{\text{slope}} = \eta_{\text{st}}\eta_q = 0.35 \times 2 = 70\%$. This is twice the value predicted by (4). $\eta_q = \Sigma_{z=0}^{\infty} 2^{-z} = 2$ originates from the fact that one of each two excitations that populate the $^4I_{13/2}$ lower laser level via stimulated emission is upconverted and contributes to lasing again. Calculation of (17) with the W_{11} and W_{22} parameters from Table I(a) results in $\eta_{\text{slope}} = 62\%$ for $LiYF_4$. The reduction in slope efficiency originates from losses via upconversion W_{22}.

Because of the recycling mechanism, the intrinsic lifetime τ_1 of the $^4I_{13/2}$ lower laser level should be as long as possible [10], [21] in order not to compete with the recycling process. Consequently, the quenching of τ_1 neither by energy transfer to a codopant [22] nor by cascade lasing on the 1.5-μm transition into the ground state [23] can improve the laser slope efficiency.

A computer simulation is performed with the above parameters but including the whole erbium rate-equation system up to the $^4F_{7/2}$ level [10] and additionally considering parameters for the inverse interionic processes that may differ from the parameters of the normal processes [20]. The cross section of ESA from the $^4I_{11/2}$ upper laser level at 970 nm (see Fig. 1) is assumed to be equal to the GSA cross section. This generally reflects the spectroscopic results [12], [24]. The calculated slope efficiency depends on the radii of pump and laser beam, see Fig. 4. The dependence is weak for radii between 50 and 15 μm as confirmed in our experiment, because the influence of ground-state bleaching and ESA from the $^4I_{11/2}$ upper laser level increase with tighter pump focus and counteract the effect of increased upconversion from the $^4I_{13/2}$ lower laser level. Thus, the slope efficiency under Ti:sapphire pumping (this paper) is not enhanced by the tighter focus but mainly by the circular pump-beam shape and better overlap with the laser mode compared to pump excitation using laser diodes with small emission zones [3]. Generally, a high pump intensity which in this case is obtained by a tight pump focus (see Fig. 4) or a small dopant concentration (cf. [20]) favor the occurrence of ground-state bleaching and draw the behavior of the erbium crystal laser toward the excited-state-absorption domain. This domain is typical of low-doped fiber lasers and will be discussed in Section V.

For a pump-beam waist of 40 μm which corresponds to our experiment $\eta_{\text{slope}} = 56\%$ is obtained for $LiYF_4$. This is the theoretical limit including all important excitation and relaxation processes of the erbium level scheme. The reduction to 56% in the simulation compared to 62% obtained from the simple model is mostly due to the fluorescences and multiphonon relaxations from the laser levels as well as the

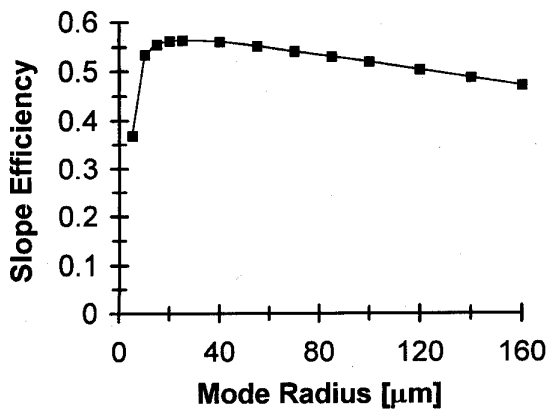

Fig. 4. Calculated limit of the slope efficiency versus mode radius for the parameter set of Er^{3+}:$LiYF_4$. Cylindrical pump and laser beams with equal radii and homogeneous photon densities are assumed. The decrease of the slope efficiency under tight focusing of the pump beam is due to significant ground-state bleaching and a dramatically increased ESA rate from the $^4I_{11/2}$ upper laser level. In crystals, the absorption lines are narrow. This implies a strong wavelength dependence of the influence of ESA under tight pump focusing.

cross-relaxation process ($^4I_{9/2}$, $^4I_{15/2} \rightarrow {}^4I_{13/2}$, $^4I_{13/2}$) which is the inverse process of interionic upconversion from the $^4I_{13/2}$ lower laser level. In our simulation, these processes contribute to the population mechanisms with a significance of approximately 10% of the pump rate.

The values of interionic processes are very difficult to determine and the calculated slope efficiency, therefore, has a relatively high error margin. Since the error margins of the measured interionic processes are not indicated in [17], we can only estimate that this error may approach several percent.

The theoretical limit neglects resonator losses L from scattering, diffraction, and water absorption as well as a nonoptimal overlap $\eta_m < 1$ between pump and laser mode and nonoptimized mirror transmissions. These effects reduce the observed slope efficiency to $\eta_{\text{slope}} = 40\%$ in our experiment.

V. Fiber Hosts: Excited-State-Absorption Domain

The investigations of Section III have shown that ESA dominates the population dynamics of low-doped erbium 3-μm fiber lasers. These processes have a completely different influence on pump wavelength and slope efficiency than interionic processes.

In erbium-doped fibers, the 791-nm pump power is absorbed on the three transitions indicated in Fig. 2. Without colasing at 1.7 μm mainly pump photons absorbed from the ground state are converted into laser photons. The strong ESA from the $^4I_{13/2}$ level at 791 nm [25] depletes the lower laser level. Subsequent ground-state fluorescences at 550 nm ($^4S_{3/2}$) and 650 nm ($^4F_{9/2}$) reduce the ground-state bleaching and the bottleneck induced by the long lifetimes of the $^4I_{11/2}$ and $^4I_{13/2}$ levels. However, the ESA populates the $^4S_{3/2}$ and leads to laser emission at 850 nm on the transition $^4S_{3/2} \rightarrow {}^4I_{13/2}$. Thus, the 2.7-$\mu$m output saturates [8].

In the cascade-lasing regime, the 850-nm transition is suppressed, and the output saturation at 2.7 μm is avoided [4]. Pump photons that are absorbed from the ground state or from the $^4I_{13/2}$ lower laser level contribute to lasing, see Fig. 2. Pump power absorbed from the $^4I_{11/2}$ upper laser level is lost. With (6), the excitation efficiency is

$$\varepsilon = \varepsilon_0 + \varepsilon_1 = (\sigma_0 N_0 + \sigma_1 N_1)/(\sigma_0 N_0 + \sigma_1 N_1 + \sigma_2 N_2). \quad (18)$$

In the ideal case, each of these pump photons is converted into one laser photon. With X from (15), this results in

$$c\phi = 2\ell X(R_0 + R_1). \quad (19)$$

Including (7) and (16), we obtain for the slope efficiency

$$\eta_{\text{slope}} = dP_{\text{out}}/dP_{\text{abs}} = (\lambda_p/\lambda_l)TX\varepsilon. \quad (20)$$

The GSA cross section at 791 nm has been measured. The ESA cross sections are obtained from a computer simulation [8]. Values are given in Table I(a). The ground-state bleaching has been measured [8]. Under 791-nm pumping, a constant fraction of 40% of the ions remain in the ground state if the pump power is more than some 20% above threshold. The $^4S_{3/2}$ level is efficiently depopulated by colasing on the 1.7-μm transition. Other levels have short lifetimes due to multiphonon relaxations. Thus, the other 60% of the ions are mostly distributed in the $^4I_{11/2}$ and $^4I_{13/2}$ laser levels of the 2.7-μm transition. The population densities of these levels are given by the combination of (12) and (13) and the measured value of N_0. Since the Stark-level structures of the $^4I_{11/2}$ and $^4I_{13/2}$ levels of erbium in fluoride fibers are not known, the Boltzmann factors of Er^{3+}:$LiYF_4$ are assumed for the calculation of (13). With the values of Table I(a), the relative population densities of the important levels are $N_2 = 22\%$, $N_1 = 38\%$, and $N_0 = 40\%$. With the cross sections from Table I(a), this results in $\varepsilon_0 = 0.31$, $\varepsilon_1 = 0.62$, and $\varepsilon = 0.93$ in (18). The losses owing to ESA from the $^4I_{11/2}$ level are thus approximately 7% of the pump power. Equation (20) then predicts a theoretical limit for the slope efficiency under 791-nm pumping of $\eta_{\text{slope}} = 27\%$. The error margin of this result is estimated to be $\pm 1.5\%$.

Our experimental approach (Fig. 3) results in $\eta_{\text{slope}} = 23\%$ which is close to the limit. The efficiency ε_1 is very high due to the high absorption cross section σ_1. Thus, the cascade-lasing regime indicated in Fig. 2 dramatically enhances the slope efficiency of the erbium 3-μm fiber laser. Without cascade lasing, approximately 20% of the excitation accumulate in the $^4S_{3/2}$ level [8]. This leads to $N_2 = 15\%$, $N_1 = 25\%$, and $N_0 = 40\%$. Only $\varepsilon_0 = 0.40$ would contribute, and the slope-efficiency limit of (20) reduces to $\eta_{\text{slope}} = (\lambda_p/\lambda_l)\varepsilon_0 = 12\%$. Experimentally obtained slope efficiencies in the normal regime range from 7–10% [13]–[16] which is again close to the predicted limit. This indicates that (20) is a good approximation.

Other pump wavelengths are not as efficient as $\lambda_p = 791$ nm. Tuning the pump to the longer wavelength side within the 800-nm pump band turns the pump wavelength away from the 791-nm peak of ESA from the $^4I_{13/2}$ lower laser level [25] and additionally results in a significantly increased ESA cross

section σ_2 from the $^4I_{11/2}$ upper laser level [26]. This reduces the excitation efficiency ε of (18) and the slope efficiency of (20). Pumping at 970 nm increases the stokes efficiency to $\eta_{st} = \lambda_p/\lambda_l = 35\%$. However, there is no ESA from the $^4I_{13/2}$ level that could deplete the lower laser level whereas ESA from the $^4I_{11/2}$ level is much stronger in this pump band [12], [24] than at 791 nm. First, this ESA efficiently depletes the upper laser level and is, therefore, detrimental to lasing. Second, pump photons absorbed from the upper laser level are not converted into laser photons. This ESA, therefore, strongly decreases the efficiency ε of (18), because σ_2 is large whereas σ_1 is zero. The enhanced stokes efficiency cannot compensate for the reduction of the excitation efficiency ε in (20). Switching the pump wavelength to the visible region reduces the stokes efficiency λ_p/λ_l. This scenario shows that pumping around 791 nm is the best choice, and the cascade-lasing regime of Fig. 2 is the most efficient pumping scheme that can be obtained.

Also, in fluorozirconate fibers, the quenching of τ_1 by either energy transfer to a codopant [27] or by cascade lasing on the 1.5-μm transition into the ground state [28] has been investigated. Energy recycling via upconversion is not present in low-doped fiber hosts. In the normal-lasing regime, the quenching of τ_1 is now favorable [10], and the laser performance is slightly improved [27], [28]. In the more efficient cascade-lasing regime of Fig. 2, a lower performance is predicted by (20) when quenching τ_1. The absorption cross section from the $^4I_{13/2}$ lower laser level is higher than from the ground state. Energy transfer from the lower laser level to the ground state, therefore, reduces the pump absorption on transitions that contribute to lasing, i.e., the decrease in ε_1 is larger than the increase in ε_0.

The experimental result for the slope efficiency in the fiber is close to the theoretical limit whereas the deviation in the crystal is slightly higher. This is due to the fact that losses in the crystal are mainly introduced by a nonoptimal overlap between pump and laser mode which reduces the slope efficiency versus absorbed pump power. In fibers, the dominating loss occurs in the incoupling efficiency of the pump beam into the fiber which is not included, because the slope efficiency is not calculated versus input power but versus absorbed power. A difference in incoupling efficiency does, therefore, not affect the calculated limit of the slope efficiency versus absorbed pump power of 27%. This limit is defined as solely depending on the population mechanisms of the erbium system.

VI. Conclusion

We have investigated the dominant excitation mechanisms that lead to stimulated emission at 3 μm in erbium-doped materials. Their influence on pump wavelength and on the theoretical limit of the laser slope efficiency has been compared in crystal and fiber hosts.

In the presence of ion-ion interactions, direct pumping of the upper laser level is the most efficient excitation mechanism. Cross-relaxation and upconversion pumping schemes exploiting different pump wavelengths do not influence this fact. Interionic upconversion from the lower laser level, however, enhances the slope efficiency. Excited-state absorption, on the contrary, cannot enhance the theoretical limit of the slope efficiency, but it severely affects certain pump wavelengths.

In crystals, the best excitation is achieved in the 970-nm pump band. The theoretical limit for the slope efficiency is calculated to be 56% due to energy recycling via interionic upconversion. We have experimentally demonstrated a slope efficiency of 40%. A pump radius of 15–50 μm leads to an optimal exploitation of the interionic upconversion. Below 15 μm, ESA losses dramatically increase.

Erbium-doped fibers exhibit strong excited-state absorption in almost every pump band. Excited-state absorption from the upper laser level introduces severe losses at the 970-nm pump wavelength. The pump wavelength with the highest stokes efficiency that efficiently depletes the lower laser level via excited-state absorption but avoids strong excited-state absorption from the upper laser level is 791 nm. With pump excitation from the ground state and the lower laser level, in a cascade-lasing regime at 2.7 and 1.7 μm, and including the fact that a small excited-state absorption from the upper laser level is still present at 791 nm, the theoretical limit for the slope efficiency is 27%. We have experimentally obtained a slope efficiency of 23%.

References

[1] L. Esterowitz and R. Allen, "Rare earth doped IR fiber lasers for medical applications," in *Proc. SPIE Infrared Fiber Opt.*, vol. 1048, 1989, pp. 129–132.

[2] B. J. Dinerman and P. F. Moulton, "3-μm cw laser operations in erbium-doped YSGG, GGG, and YAG," *Opt. Lett.*, vol. 19, pp. 1143–1145, 1994.

[3] T. Jensen, A. Diening, and G. Huber, "A diode pumped 1.1 W cw Er:YLF laser at 2.8 μm," in *Conf. Lasers Electro-Opt.*, 1995, vol. 15, OSA Tech. Dig. Series, Opt. Soc. Amer., Washington, DC, 1995, postdeadline paper CPD29.

[4] M. Pollnau, C. Ghisler, G. Bunea, M. Bunea, W. Lüthy, and H. P. Weber, "150 mW unsaturated output power at 3 μm from a single-mode-fiber erbium cascade laser," *Appl. Phys. Lett.*, vol. 66, pp. 3564–3566, 1995.

[5] S. Nikolov, N. P. Schmitt, G. Reithmeier, and T. Halldorsson, "Fiber coupled diode pumped Er:YSGG laser at 2.8 μm," in *Laser'95 München, Kongress Lasermed*, W. Waidelich, Ed. Berlin: Springer-Verlag, to be published.

[6] R. S. Quimby and W. J. Miniscalco, "Continuous-wave lasing on a self-terminating transition," *Appl. Opt.*, vol. 28, pp. 14–16, 1989.

[7] K. S. Bagdasarov, V. I. Zhekov, V. A. Lobachev, T. M. Murina, and A. M. Prokhorov, "Steady-state emission from a $Y_3Al_5O_{12}$: Er^{3+} laser ($\lambda = 2.94$ μ, $T = 300°K$)," Kvant. Elektr., Moscow, vol. 10, pp. 452–454, 1983; also in *Sov. J. Quantum Electron.*, vol. 13, pp. 262–263, 1983.

[8] S. Bedö, M. Pollnau, W. Lüthy, and H. P. Weber, "Saturation of the 2.71 μm laser output in erbium doped ZBLAN fibers," *Opt. Commun.*, vol. 116, pp. 81–86, 1995.

[9] R. C. Stoneman and L. Esterowitz, "Efficient resonantly pumped 2.8-μm Er^{3+}:GSGG laser," *Opt. Lett.*, vol. 17, pp. 816–818, 1992.

[10] M. Pollnau, T. Graf, J. E. Balmer, W. Lüthy, and H. P. Weber, "Explanation of the cw operation of the Er^{3+} 3 μm crystal laser," *Phys. Rev. A*, vol. 49, pp. 3990–3996, 1994.

[11] R. Spring, M. Pollnau, S. Wittwer, W. Lüthy, and H. P. Weber, "Slope efficiency of a pulsed 2.8-μm Er^{3+}:$LiYF_4$ laser," in *Adv. Solid-State Lasers Conf., Tech. Dig.*, Opt. Soc. Amer., Washington, DC, 1996, pp. 262–264.

[12] M. Pollnau, W. Lüthy, H. P. Weber, K. Krämer, H. U. Güdel, and R. A. McFarlane, "Excited-state absorption in Er:BaY_2F_8 and $Cs_3Er_2Br_9$ and comparison to Er:$LiYF_4$," *Appl. Phys. B*, to be published.

[13] H. Yanagita, I. Masuda, T. Yamashita, and H. Toratani, "Diode laser pumped Er^{3+} fiber laser operating between 2.7–2.8 μm," *Electron. Lett.*, vol. 26, pp. 1836–1838, 1990.

[14] L. Wetenkamp, "Efficient cw operation of a 2.75 μm Er^{3+}-doped fluorozirconate fiber laser pumped at 650 and 795 nm," *Archiv für Elektronik und Übertragungstechnik*, vol. 45, pp. 328–331, 1991.
[15] C. Frerichs, "Efficient Er^{3+}-doped CW fluorozirconate fiber laser operating at 2.7 μm pumped at 980 nm," *Int. J. Infrared and Millimeter Waves*, vol. 15, pp. 635–649, 1994.
[16] S. Bedö, W. Lüthy, and H. P. Weber, "Limits of the output power in Er^{3+}:ZBLAN single-mode fiber lasers," *Electron. Lett.*, vol. 31, pp. 199–200, 1995.
[17] H. Chou and H. P. Jenssen, "Upconversion processes in Er-activated solid state laser materials," *Tunable Solid State Lasers*, vol. 5 OSA Proc. Series, M. L. Shand and H. P. Jenssen, Eds., Opt. Soc. Amer., Washington, D.C., pp. 167–174, 1989.
[18] S. A. Pollack, D. B. Chang, and N. L. Moise, "Upconversion-pumped infrared erbium laser," *J. Appl. Phys.*, vol. 60, pp. 4077–4086, 1986.
[19] P. Xie and S. C. Rand, "Continuous-wave, pair-pumped laser," *Opt. Lett.*, vol. 15, pp. 848–850, 1990.
[20] M. Pollnau, W. Lüthy, and H. P. Weber, "Population mechanisms of the green Er^{3+}:$LiYF_4$ laser," *J. Appl. Phys.*, vol. 77, pp. 6128–6134, 1995.
[21] V. Lupei, S. Georgescu, and V. Florea, "On the dynamics of population inversion for 3 μm Er^{3+} lasers," *IEEE J. Quantum Electron.*, vol. 29, pp. 426–434, 1993.
[22] D. S. Knowles and H. P. Jenssen, "Upconversion versus Pr-deactivation for efficient 3 μm laser operation in Er," *IEEE J. Quantum Electron.*, vol. 28, pp. 1197–1208, 1992.
[23] B. Schmaul, G. Huber, R. Clausen, B. Chai, P. LiKamWa, and M. Bass, "Er^{3+}:$YLiF_4$ continuous wave cascade laser operation at 1620 and 2810 nm at room temperature," *Appl. Phys. Lett.*, vol. 62, pp. 541–543, 1993.
[24] T. Danger, J. Koetke, R. Brede, E. Heumann, G. Huber, and B. H. T. Chai, "Spectroscopy and green upconversion laser emission of Er^{3+}-doped crystals at room temperature," *J. Appl. Phys.*, vol. 76, pp. 1413–1422, 1994.
[25] L. Esterowitz, R. Allen, and I. Aggarwal, "The effects of excited-state absorption on the cw operation of the erbium $^4I_{11/2} \rightarrow {}^4I_{13/2}$ fiber laser," in *Adv. Solid-State Lasers, 1991*, Tech. Dig. Series, Opt. Soc. Amer., Washington, DC, 1991, pp. 160–162.
[26] M. Pollnau, E. Heumann, and G. Huber, "Time-resolved spectra of excited-state absorption in Er^{3+} doped $YAlO_3$," *Appl. Phys. A*, vol. 54, pp. 404–410, 1992.
[27] J. Schneider, D. Hauschild, C. Frerichs, and L. Wetenkamp, "Highly efficient Er^{3+}:Pr^{3+}-codoped cw fluorozirconate fiber laser operating at 2.7 μm," *Int. J. Infrared and Millimeter Waves*, vol. 15, pp. 1907–1922, 1994.
[28] J. Schneider, "Mid-infrared fluoride fiber lasers in multiple cascade operation," *IEEE Photon. Technol. Lett.*, vol. 7, pp. 354–356, 1995.

M. Pollnau, photograph and biography not available at the time of publication.

R. Spring, photograph and biography not available at the time of publication.

Ch. Ghisler, photograph and biography not available at the time of publication.

S. Wittwer, photograph and biography not available at the time of publication.

W. Lüthy, photograph and biography not available at the time of publication.

H. P. Weber (M'72–SM'85–F'89) photograph and biography not available at the time of publication.